Preparation and characterization of La-doped and La-dispersed barium hexaferrite

A dissertation submitted in partial fulfillment of the requirement for the award of degree of

Master of Technology

In

MATERIALS AND METALLURGICAL ENGINEERING

Submitted By

Deepshikha Shekhawat
(Roll No. 601202003)

Under the supervision of

Dr. Puneet Sharma
Associate Professor

SCHOOL OF PHYSICS AND MATERIALS SCIENCE
THAPAR UNIVERSITY
PATIALA – 147004
July 2014

CERTIFICATE

I hereby certify that the thesis entitled," **Preparation and characterization of La-doped and La-dispersed barium hexaferrite",** is an authentic record of my own work carried out as the requirements for the award of degree of Master of Technology (Materials & Metallurgical Engineering) submitted in School of Physics & Material Science (SPMS), Thapar University, Patiala, under the supervision of **Dr. PUNEET SHARMA** during January to June 2014. The matter presented in this thesis has not been submitted to any other University or institute for the award of any degree.

15/7/14
Dated:

(Deepshikha Shekhawat)

Roll. No. 601202003

This is to certify that the above statement made by the candidate is correct and true to the best of my knowledge.

(Dr. Puneet Sharma)

Associate Professor
School of Physics and Materials Science
Thapar University
Patiala.

Countersigned by:

(Dr. Kulvir Singh)
Head
SPMS,
Thapar University
Patiala.

(Dr.S.K.Mohapatra)
Dean (Academic Affairs)
Thapar University
Patiala.

ACKNOWLEDGEMENT

First of all I would like to thank the almighty, who has always guided me to work on the right path of the life.

This work would not have been possible without the encouragement and guidance of my supervisor **Dr. Puneet Sharma**. I am extremely thankful to my supervisor for their time, patience, discussions and valuable comments. Their enthusiasm and optimism made this experience both rewarding and enjoyable.

I am equally grateful to **Dr. Kulvir Singh**, Professor and Head, SPMS, for motivation and inspiration that triggered me for the thesis work.

I am also thankful to **Mrs. Samiksha Verma,** Research Scholar for her encouragement and execution of report work and providing me invaluable support and training in various techniques and uses of equipment.

My special thanks to P.G. Lab Incharge **Mr. Purushottam** and **Mr. Jant Singh**, for their all kind of help in PG Lab for creating a healthy research environment.

I would like to give my special thanks to Research Scholars Samita Thakur, Mintu Tyagi, Satwindar Deniwal, Sakshi Gupta and Chandni khurana and my Classmates for helping me at various stages of my experimental work.

I want to thank entire faculty and staff members of SPMS for their direct-indirect help, cooperation, love and affection, which made my stay at Thapar University memorable.

Last but not least, I would like to thank my parents for their wonderful love and encouragement. Without their blessings none of this would have been possible. I would also like to thank my close friends for their constant support.

Deepshikha Shekhawat

(601202003)

TABLE OF CONTENTS

LIST OF FIGURES

LIST OF TABLES

MOTIVATION

Among the M-type hard ferrites, barium ferrite ($BaFe_{12}O_{19}$) have greatest technology interest due to its low cost and moderate magnetic properties. Magnetic properties can be tailored by changing processing condition and by suitable cationic substitution Ba or Fe site. Various rare earth substitutions have been tried at Ba site which include La, Gd, Nd, Sm etc. However it is uncertain that the cation completely substituting the Ba or remain in free oxides form in the system, therefore, to resolve this ambiguity rare earth oxide La_2O_3 is doped and dispersed in $BaFe_{12}O_{19}$, it effect in the magnetic properties can be compared. Moreover, the site preference of substituted cation can also be understood.

ABSTRACT

In the present work Lanthanum substituted and Lanthanum dispersed barium hexaferrite ($BaFe_{12}O_{19}$) were prepared by solid state synthesis method. The structural, magnetic and microstructural characterization were carried out by X-ray diffractometer, VSM, mössbaure spectroscopy and scanning electron microscope respectively. XRD pattern shows the single phase $BaFe_{12}O_{19}$ for La-doped samples, whereas for La-dispersed samples, barium monoferrite ($BaFe_2O_4$) was found as a secondary phase with major phase $BaFe_{12}O_{19}$. Crystallite size was calculated by Debye sherrer formula. SEM shows that the average particle size of powder were same for La-doped and La-dispersed $BaFe_{12}O_{19}$. The magnetic properties show the variation in coercivity and saturation magnetization. Coercivity found to decrease in La-dispersed samples. However, no variation was observed in La-doped samples. Saturation magnetization found to decreased for La-doped barium hexaferrite, however in La-dispersed samples saturation magnetization first decreases and then increased to the value of pure $BaFe_{12}O_{19}$.

CHAPTER-1 INTRODUCTION

1 Ferrites:

Ferrites are essentially magnetic ceramics, made by oxides of iron and other metals. The term ferrite is commonly used to describe a class of insulating magnetic oxide compounds, which contains iron oxide as a principal component such as hematite (Fe_2O_3), magnetite (Fe_3O_4) as well as oxides of other metals [1]. Ferrites are, like most other ceramic hard and brittle.

Ferrites can be classified according to magnetic behavior and crystal structure.

1.1 Classification according to magnetic behavior: according to magnetic behavior, ferrites can be classified into two types.

Soft ferrites:

Soft ferrites can be easily magnetized and demagnetized. They retain their magnetization only in the presence of magnetic field. They have narrow hysteresis loop. An ideal soft ferrites have low coercivity (H_c), large saturation magnetization (M_s), zero remanence (B_r), zero hysteresis loss, and large permeability. Hysteresis loop of soft ferrite is shown in figure 1.1. The area within a loop represents a magnetic energy loss per unit volume of material [2]. Soft ferrites are used in various field where we require the low energy losses for example, transformer cores. Few important soft ferrites are $MnZnFe_2O_4$, $NiZnFe_2O_4$ etc.

Hard ferrites:

Hard ferrites are hard to magnetized and demagnetize, even when the magnetizing force is removed a substantial magnetic flux density remains. These ferrites have high saturation magnetization (M_s), high magnetocrystalline anisotropy (H_A), high maximum energy product $(B_H)_{max}$ and high coercivity (H_c) and suitable candidate for permanent

magnets [3]. Hard ferrites have rectangular hysteresis loop [4]. Among the permanent magnets the most important materials are alnico, hard ferrites, samarium cobalt and neodymium iron boron. But hard ferrites are found to be most suitable then other materials due to low production cost and excellent magnetic properties. Few important hard ferrites are $SrFe_{12}O_{19}$, $BaFe_{12}O_{19}$, and $CoFe_2O_4$ etc.

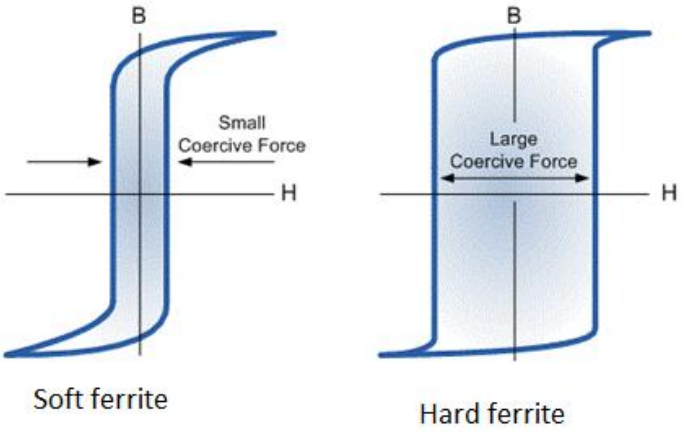

Figure 1.1 Hysteresis loop for soft and hard ferrites

1.2 Classification according to crystal structure: According to crystal structure ferrites are divided into three types. These are mainly distinguished with the ratio of the Fe_2O_3 from other oxides. Different types of ferrites according to crystal structure as illustrated in table 1.1.

Table 1.1 Different types of ferrites according to crystal structure.

Type	Structure	Formula	Example
Spinel	Cubic	MFe_2O_4	M=Cd,Co,Mg,Mn,Cu,Fe,Ni and Zn
Garnet	Cubic	$RE_3Fe_5O_{12}$	RE=Y,Sm,Eu,Gd,Tb,Dy,Ho and Lu
Magnetoplumbite	Hexagonal	$MFe_{12}O_{19}$	M=Ba,Sr and Pb

Spinel:

Spinel ferrites are also known as cubic ferrites. Chemical formulas of these ferrites are represented by: $Me^{+2}O.Fe^{+3}{}_2O_3$, where; Me represents divalent magnetic ions and Fe can be replaced by other trivalent magnetic ions, in a cubic structure. Divalent metal cations occupy 8 out of the possible 64 *A*-tetrahedral sites and trivalent metal ions occupy 16 out of possible 32 *B*-octahedral sites. Oxygen anions make a close packed structure and all these contribute 32 ions that electrically balance the unit cell [5]. The magnetism in these structures arises from a super exchange mechanism and the net moment is given by the sum of individual moments of all sites. Figure 1.2 shows the cation distribution in a spinel crystal structure.

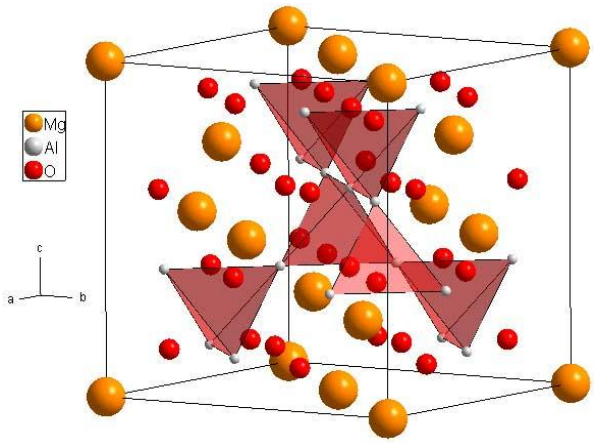

Figure 1.2 Crystal Structure of Spinel Ferrite

The most popular example and abundant of the magnetic spinels is magnetite, Fe_3O_4 [6]. The spinel structure is cubic structure and as a result the magnetocrystalline anisotropy energy is relatively small then the other structures and the corresponding magnetic anisotropy fields (H_A) are typically 10s of Oe.

Garnet:

Garnet ferrites have the chemical formula $M^{+3}{}_3Fe^{+3}{}_2(Fe^{+3}O_4)_3$, in which M is rare earth oxides and similarity to spinels, grow in cubic crystal structure. The unit cell consists of twenty four Fe^{+3} ions at tetrahedral sites (A), sixteen Fe^{+3} ions at octahedral sites (B) and 24 M^{+3} ions at the dodecahedral sites (C). Metals ions have +3 state and the oxygen

sublattices of garnets structure are completely filled. Figure 1.3 shows the crystal structure of the most famous garnet, yttrium iron garnet (YIG) [7]. In the garnet unit cell all possible cation positions are filled dominating to uncommon chemical and structural stability as well as high insulating properties. YIG ($Y_3Fe_5O_{12}$) has a high Verdet constant, which responsible for a large magneto-optical response and high Q factor at microwave frequencies. YIG is used in radio frequency, microwave, optical, and magneto-optical applications.

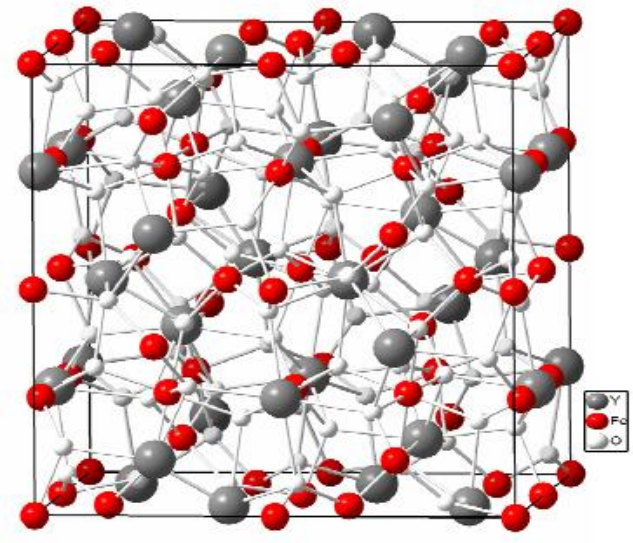

Figure 1.3 Crystal Structure of Garnet

Hexaferrites:

The hexaferrites have hexagonal closed packed crystal structure which leading to high magnetocrystalline anisotropy and magnetic anisotropy fields and subsequently high FMR frequencies [8]. Hexaferrite further divided on the basis of different crystal structures and oxygen stoichiometry. Hexagonal (magnetoplumbite) structure can be classified as M-, U-,W-, X-,Y-,Z- type ferrite are shown in a following table 1.2.

Table 1.2 Types of Hexaferrite [9-10]

Types	Chemical Formula	
M-	$RFe_{12}O_{19}$	R = Ba, Sr, Pb
U-	$R_4Co_2Fe_{36}O_{60}$	Me = Fe^{+2}, Ni^{+2}, Mn^{+2} etc
W-	$RMe_2Fe_{16}O_{27}$	
X-	$R_2Me_2Fe_{28}O_{46}$	
Y-	$R_2Me_2Fe_{12}O_{22}$	
Z-	$R_3Me_2Fe_{12}O_{41}$	

Among all the hexagonal ferrites, M type ferrite $BaFe_{12}O_{19}$ or shortly "BaHF" or BaM have of greatest technological interest. Due to high value of permeability (necessarily >1), high value of magnetization and good dielectric properties these properties make them special candidates for radar absorbing materials at microwave frequencies. M- type hexaferrite can easily saturate along the c axis, whereas Y- and Z- type hexaferrite saturated along its basal plane by applied field.

1.3 M-type ferrites:

M-type ferrite has the formulae of $BaO.6Fe_2O_3$ (BaM), $SrO.6Fe_2O_3$ (SrM) and $PbO.6Fe_2O_3$ (PbM). M-type ferrites are mainly used as permanent magnet, once they get magnetized, have strong resistance to demagnetizing field.

Crystal structure, magnetic structure and phase diagram of M-type ferrites:

Barium hexaferrite is isostructural with naturally occuring magnetoplumbite with a space group of P63/mmc. Figure 1.4 shows the unit cell of barium hexaferrite [11]. One unit cell of barium hexaferrite consists of two formula units. In the unit cell, the O^{-2} ions form a hexagonal close packed lattice. Every five oxygen layers, one O^{-2} ion is replaced with Ba^{+2} due to the similarity of their ionic radii. The structure is build up from smaller unit: a cubic block S, having the spinal structure and a hexagonal block R, containing Br^{+2} ions [12-13]. Five Oxygen layers make one formula unit and RSR*S* make one unit cell.

These two formula units show 180^0 rotational symmetry around the hexagonal *c*-axis against the lower or upper molecule. The O^{-2} layer containing Ba^{+2} is a mirror plane being perpendicular to the *c*-axis. Fe^{+3} ions occupy interstitial positions at different crystallographic sites i.e. tetrahedral ($4f_1$), octahedral (12*k*,2a,2b) and trigonal bi-pyramidal ($4f_2$) sites of oxygen lattice. From magnetic consideration M-type compounds have a typical ferromagnetic structure [13]. Barium hexaferrite shows the magnetism due to ferric ions and each ferric ion have 5μB magnetic moment.

M-type (a) crystal structure showing the S and R units where ○ is O^{-2}; ● is Ba^{+2}; and ■, ✧, •, **O** and all Fe^{+3} at $4f_1$, 2b,12k,$4f_2$, and 2a positions respectively. In magnetic structure, the arrows represent size and spin direction of unpaired electron at various crystallographic positions. The total magnetization at temperature T can be expressed as:

$$Js(T) = 6\sigma_K(T) - 2\sigma_{f1}(T) - 2\sigma_{f2}(T) + \sigma_b(T) + \sigma_a(T)$$

Where σ_k, σ_{f1},σ_{f2},σ_b,σ_a represents the magnetization of one Fe^{+3} ion in each sub lattice. Opposite spin interacts and cancel out to each other, so the net magnetic moment calculated at 0K is 20μB for each formula unit.

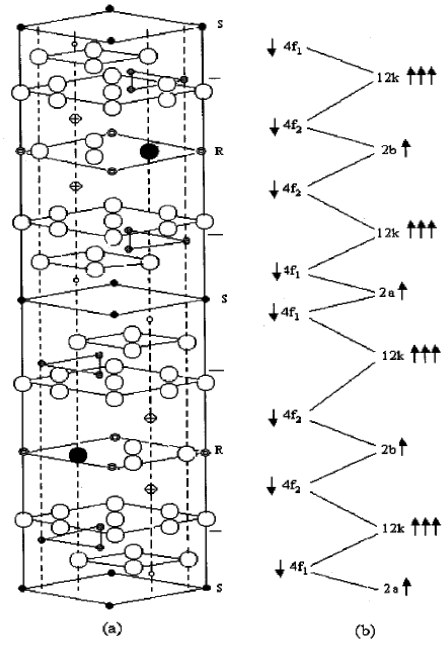

Figure 1.4 (a) Crystal Structure and (b) Magnetic Structure

Table 1.3 Summary of the crystal structure and magnetic structure

Sub lattice	Co ordination	Number of ions	Spin
12*k*	Octahedral	6	Up
$4f_1$	Tetrahedral	2	Down
$4f_2$	Octahedral	2	Down
2a	Octahedral	1	Up
2b	Fivefold (Trigonal bi-pyramid)	1	Up

Figure 1.5 shows the phase diagram of BaO and Fe_2O_3 system. In the phase diagram the homogeneity range is very narrow and in the eutectic range somewhat enlarged, at most towards the side rich in the BaO [14]. Towards higher temperature range, incongruent melting occur at 1448 ^oC (1 bar O_2) and 1390 ^oC (air), with the W phase $BaFe_{18}O_{27}$ (= BaO $2FeO.8Fe_2O_3$) is formed. However, in vacuum anneling above 1100 ^oC, Fe_3O_4 and S_7F_5 phase is formed with the release of oxygen, where S= $2(BaO.Fe_2O_3)$ and F= $BaO.6Fe_2O_3$ or $BaFe_{12}O_{19}$ phase is stable only towards lower temperature range. Towards the Fe_2O_3 richer side the two phase region ($BaFe_{12}O_{19}$+Fe_2O_3) are formed. On the BaO richer region, the phase S_7F_5 and S_3F_2 are the neighboring phases both of them being very close to the composition S_4F_3 [15]. The eutectic temperature of 1210 ^oC (1 bar O_2) or 1195 ^oC (air) as well as the eutectic content of 53.5 or 55 mole % are close to one another.

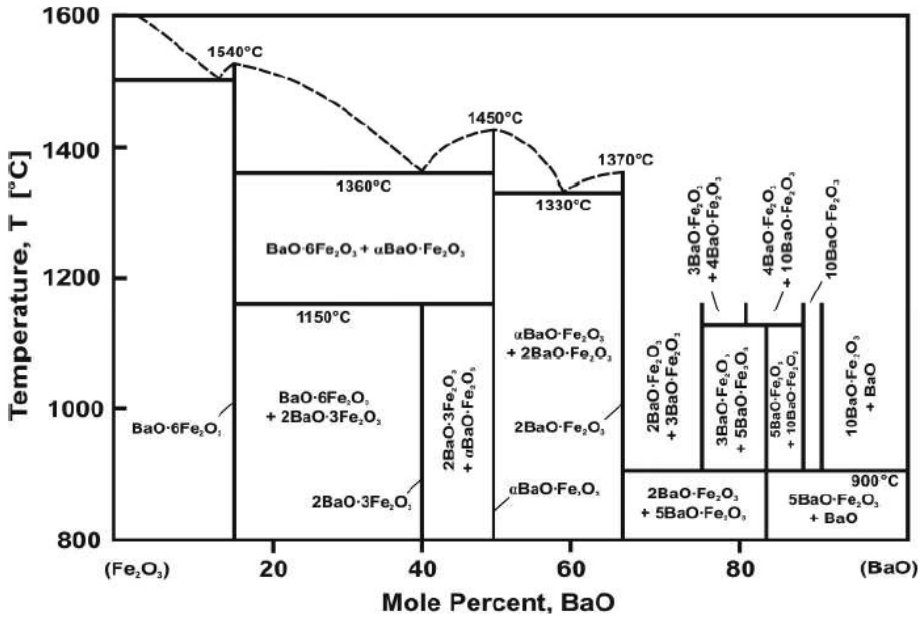

Figure 1.5 Phase diagram of Fe_2O_3-BaO system

1.4 Processing methods:

There are various type of method to process hard ferrites which are:

1.4.1 High energy ball milling (HEBM):

Ball mill is a good tool for grinding many materials into fine powder. There are two type of grinding: the dry process and the wet process. It can be divided into tabular type and following type according to different forms of discharging material. After the grinding the state of the solid is charge i.e. size and shape of grain. The ball mill is a key equipment for grinding [14]. It is widely used for the cement, the silicate product, new type building material, fine-proof material, chemical fertilizer, black and non-ferrous metal, glass, ceramics and etc.

1.4.2 Chemical Co-precipitation:

Co-precipitation (CPT) is carrying down by a precipitate of substances normally soluble under the conditions employed. In medicine, co-precipitation is specifically the precipitation of an unbound “antigen along with an antigen-antibody complex” [16]. There are three main mechanisms of co-precipitation: inclusion, occlusion, and

adsorption. An inclusion occurs when the impurity occupies a lattice site in the crystal structure of the carrier, resulting in a crystallographic defect. This can happen when the ionic radius and charge of the impurity that is weakly bound (adsorbed) to the surface of the precipitate [17]. An occlusion occurs when an adsorbed impurity get physically trapped inside the crystal as it grows.

1.4.3 Sol-Gel Method:

In this method, the 'sol' gradually evolves towards the formation of gel-like diphase system containing both a liquid phase and solid phase whose morphologies range from discrete particles to continuous particles. In the case of the colloid, the volume fraction or density of paticles may low that a significant amount of the fluid may need to be removed initially for the gel-like properties to be recognized [18]. To removing the remaining liquid phase, apply the drying process. The rate at which the solvent can be removed is ultimately determined by the distribution of porosity in the gel. The microstructure of the final component will clearly be strongly influenced by changes imposed upon the structural template during this phase of processing. After this, a thermal treatment or firing process is necessary for further poly condensation. When we do the final sintering, we found enhance mechanical properties, structure stability, densification and grain growth. The sol-Gel technique is a cheap and low temperature technique that allows for the fine control of the product's chemical composition. Sol-Gel derived materials have diverse applications in optics, electronics, energy, space etc [19].

1.4.4 Solid state reaction method:

Among the various processing method solid state synthesis is widely used. The solid state synthesis is basically a diffusion method. This method starts with mixing of raw materials can take place either with a wet or dry process. In wet mixing, generally using an aqueous suspension, vibration drum or agitator mills are used [20]. This mixing method is extremely effective but dewatered either mechanically, e.g., in a filter press and then dried. Dry mixing is done either by grinding and mixing in drum or ball mills or intensive mixing in an edge runner mill or in high intensity counter flow mixer with swirler. The

calcinations temperature also plays an important role in the formation of hexaferrite phase.

1.5 Applications of Hexaferrite:

As we have mention, ferrite materials possess moderate to high magnetization, high permeability, high permittivity, and high electrical resistivity, that they are uniquely suited for high frequency applications over many decades of frequency. At lower frequencies, ferrites commonly used as inductor cores in power generation, conditioning, and conversion, while at higher frequencies. They are used in passive and active devices that send, receive and manipulate electromagnetic signals [21]. Other applications include EMI shielding and microwave absorbers military search radar, military radar, missile radar, cellular mobile radar, satellite communication uplink and downlink, automobile anti-collision radar, oceanographic radar, space telemetry etc.

Military Radar

Missile Radar

Space Telemetry

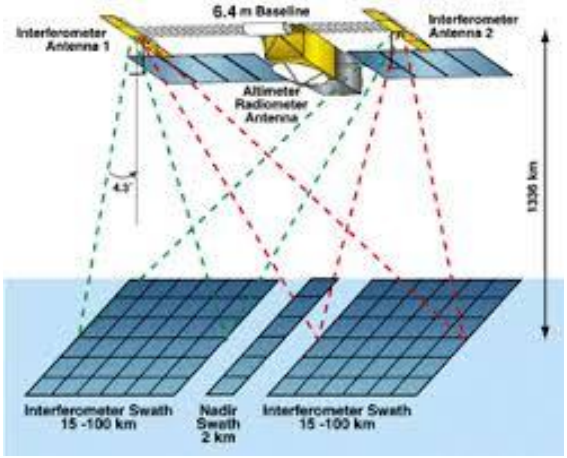

Oceanographic Radar

Figure 1.6 Several applications of hard magnetic materials

CHAPTER-2 LITERATURE REVIEW

In the past few years hexaferrites has gained considerable attention due to good magnetic properties, high packing density at low cost. They have been used regularly in studies from 1931, however they found popularity recently due to its use in magnetic card strips, speakers, and magnetic tapes. One area in particular it has found success in long-term data storage material, extremely resistant to temperature, corrosion, and oxidization.

A lot of work has been carried out to prepared barium hexaferrite from various methods, and effect of various cationic substitution on the magnetic and structural properties has been studied. The few important work has been summarized below:

H. Sozeri *et al.* [22] prepared the La substituted barium hexaferrite {($Ba_{1-x}La_x$) Fe_2O_3, where $0<x<1$ and $1<n<6$)} at 800 to 1200 ^oC. They determine the effect of lanthanum substitution on the phase composition, lattice parameter and magnetic properties of barium hexa ferrite. They observed the lattice parameters, both '*a*' and '*c*' decreases with increasing La amount, which further decreases the unit cell volume. Scanning electron microscope micrographs shows the pure and La-substituted sample have grain size smaller than the 1 mm. Coercivities of the La-substituted sample increase with increasing La amount and reaches to a maximum value of 5.73 KOe, for x=0.3.

R. M. Kershi *et al*. [23] prepared nanocrystalline La doped barium W-type hexagonal ferrites using ceramic technique. They investigated the main structural parameters of the samples such as cell parameters, crystallite size and lattice strain. They observed that the fractional changes in cell parameters with La-doping and get the linear relationship between average crystallite size and average lattice strain with La content.

P. Sharma *et al.* [24] prepared two series of barium hexaferrite one by mechanical alloying and other by conventional route. A reduction in phase formation temperature is found as compared to conventional prepared powder. They observed the higher amount of hexaferrite phase formed in the mechanically processed samples, have the higher saturation magnetization and remenence. They founded that coercivity enhancement in

the mechanically alloyed samples is attributed to its smaller particle size as compared to the conventionally prepared samples.

M. Radawan *et al*. [25] prepared the barium hexaferrite nanoparticles by chemical coprecipitation by calcined at different temperature. They studied the effect of Fe/Ba molar ratio. Observed that when the addition of surfactants, enhanced the formation of single phase barium hexaferrite at low calcinations temperature and found it was also helpful in controlling microstructure.

Y. Chen *et al*. [26] synthesized the one-dimensional nanomaterial using high-energy ball milling. They used two different types of HEBM mills: a vertical rotating ball mill and a planetary ball mill. They observed the HEBM has played an important role in the formation of the nanotubes and nanowires, and conclude that HEBM creates a nanosized, disordered and more active structure in the precursor materials.

A. Ghasemi *et al*. [27] prepared the doped barium hexaferrite and analyzed the electromagnetic properties and microwave absorbing characteristics. They observed that the grain size was almost depend on the chemical composition. They found, samples having higher magnetic susceptibility, higher permeability, larger coercive force and large hysteresis loop shows the larger microwave-absorbing ability. They conclude that it could be used in the application of microwave absorbers over 15 GHz, and with satisfactory reflection losses, at a thickness of 1.8 mm by controlling the substituted value of Mn, Cu and Ti elements in barium ferrite.

S. Ounnunkad *et al.* [28] studied the effect of La substitution in barium hexaferrite by citrate combustion process. They found that La-Zn substitution greatly modified the magnetic properties and microstructure of barium hexaferrite. They observed the X-ray diffraction and found, it have monophasic magnetoplumbite phase without any intermediate phase. They examined magnetic properties by VSM, it shows abnormal magnetic behavior in ferrite pellet. In the beginning the saturation magnetization increased up to maximum (x= 0.15) and then decreased dramatically. They gave the reason of decreasing of *Ms* due to a Fe^{+3}($3d^5$ high spin) ion converting into Fe^{+2} state ($3d^6$ low spin). They found, coercive field strength *(Hc)* increasing in order of ~1-2.5 KOe

with La concentration. They investigated the grain morphology, it changed from hexagonal platelet like shape to irregular shape without changing in the crystalline structure with increasing La ion.

Cong-ju Li *et al.* [29] prepared barium nanofiber from electrospinning technique by heat treatment at different temperature. They analyzed XRD and found that barium hexaferrite formed without any intermediate phase at 1100^0C. They observed that these hexagonal ferrites have quite heavy as granular material which responsible for limited application in microwave absorber and magnetic shielding materials. They analyzed that fiber are more preferable for resolving the problem of increasing specific surface area for increasing the absorbing ability per unit mass.

N. Chan *et al.* [30] prepared the lanthanum substituted M-type strontium ferrite using sol-gel method. They made $Sr_{1-x}La_xFe_{12}O_{19}$ where x=0.05 to 0.2. They analyzed the result of X-ray diffraction ,mossbauer and vector network analyzer. They observed when enhanced interface polarization and repetitious reflection it improves the microwave properties due to decreasing in grain size. Analyzed that when Lanthanum amount reaches about x=0.15 then it shows the minimum reflection loss about -41.7 db decreased by 73% and 10 db bandwidth is over 4 GHZ expanded by 50%.

R. Grossinger *et al.* [31] synthesized rare earth substitution in M-type ferrite by hydrothermal synthesis .They observed the magnetization values was almost same as that of SrM ferrite which was conformed from NMR and Mossbauer spectroscopy. On the other hand, their intrinsic corcivities increases upon doping. They found intrinsic corcevity and found that it increased without any deterioration in the magnetization or in the remanence.

D. Seifert *et al.* [32] synthesized La substituted M-type Sr hexaferrite by ceramic root. They found the stable form of $LaFe_{12}O_{19}$ with single phase at $1350^0$and 1400^0 C. They analyzed the result of X-ray powder diffraction and observed that when La concentration increases then lattice parameter varies. From magnetization measurement they observed that magnetic moment decreases with La concentration increases.

M. Kupferling *et al.* [33] prepared the La-substituted Sr hexaferrite with different La concentrations *x*. They investigated the magnetic and structural properties with the substitution. Observed that the increasing in magnetocrystalline anisotropy at low temperatures. They also observed that when La increases then '*c*' axis decreases while '*a'* is increasing slightly. They concluded the most interesting result was that the pure La hexaferrite exhibits a lattice distortion near T=100 K. This distortion takes place mainly in the basal plane of the hexagonal lattice.

V. Babu *et al.* [34] prepared the barium hexaferrites by ball milling of a BaO_2 and Fe_2O_3 mixture followed by thermal heat treatments. They investigate the structure and magnetic properties by X-ray diffraction, scanning electron microscopy and vibrating sample magnetometer techniques. They observed the effect of grain refiner and found that the hard magnetic properties were improved significantly. They conclude prepared barium hexaferrite powders by ball milling has higher coercive force than that of other barium hexaferrite.

W. Zhong *et al.* [35] synthesized the La substituted M-type strontium ferrites ($Sr_{1-x}La_xFe_{12}O_{19}$) by the sol–gel method. They observed that when x is below 0.20, then X-ray diffraction shows the single M-type hexaferrite at 850 ^oC. They also observed the magnetic properties and observed such as the saturation magnetization and the intrinsic coercivity increase with increasing the amount of La^{+3}. They analyzed that these particles are very useful for the bonded magnet materials.

F. Hu *et al.* [36] synthesized the M-type strontium ferrites with substitution of Sr^{2+} by rare-earth La^{3+} by conventional ceramic technology. They analyzed the structure, magnetic properties, and magneto-optical by x-ray diffraction (XRD), vibrating sample magnetometer (VSM), and magneto-optical ellipsometry. They have observed that single M-type hexagonal ferrites formed at 1290 ^OC for 3 h. They also investigate magnetic properties and observed values has changed due to change in valence of Fe ions which induced by substitution of La ions. Most significantly magneto-optical activity of La^{3+} substituted M-type strontium ferrites was found around 3 eV.

T.T. Viet Nga *et al.* [37] prepared the La-substituted strontium hexaferrite particles by using sol-gel method and calcined at 750°C to 1050°C for 2h. They investigated the sample by using X-ray diffraction (XRD), scanning electron microscopy (SEM) and vibrating sample magnetometer (VSM). Observed that when x = 0.1 ,0.2 then it improves the crystallinity and inhibits the grain growth of the samples in a wide range of calcination temperature. They conclude that this factor are responsible for production of high-coercivity hexaferrites by sol-gel technology.

X. Liu *et al.* [38] synthesized the La substitution in M-type strontium ferrites by the ceramic process. They investigated the XRD, VSM and Mossbauer spectrum of the sample. Observed that when the substituted amount x is below 0.30 then formed the single phase M-type hexagonal ferrites. They also observed that this amount also suitable for remarkably increases the saturation magnetization and intrinsic coercivity with the La^{3+} addition for the same sintering temperature. Intrinsic coercivity increase at first, then decrease gradually. The Curie temperature of $Sr_{1-x}La_xFe_{12}O_{19}$ decreases linearly with increasing La^{3+} substitution.

R. Nowosielski *et al*. [39] prepared iron oxide and barium carbonate mixture from milling process for 30 hours and annealed at 950 °C. They analyzed the sample by X-ray identification. Observed that sample having $BaFe_{12}O_{19}$ phase and Fe_2O_3. They concluded that rest of $BaCO_3$ dissociation in the presence of Fe_2O_3, which forms a compound of $BaFe_{12}O_{19}$.

T. Kaur *et al*. [40] they prepared the La-Ni doped barium nano hexaferrites (BaM) via sol gel citrate precursor method. Studied the effect of pH on the properties of the synthesized nano hexaferrites. They analyzed the X-ray diffraction (XRD), Fourier transform infrared spectroscopy (FTIR) and Vibrating Sample Magnetometer (VSM). They found that particle size of the doped barium nano hexaferrite decreases with increase in pH and FTIR spectra confirms the formation of hexagonal ferrites in the presence of the bands in the 375-600 cm^{-1} range. They analyzed the magnetic properties such as coerecivity, saturation magnetization, rententivity and anisotropy factor also increases with increase in pH value.

C. Doroftei *et al* . [41] synthesized the La substituted Sr hexaferrites by sol-gel selfcombustion. They annealed at different temperatures (800, 900 and 1000 ^{o}C) for various annealing times (10, 20, 40, 80, 160 and 320 minutes). They examined that *Ms* and *Mr* increase with both the annealing time and temperature. They observed that *Hc* significantly increases up to maximum value and then decreased. This variation they explained by the transition from single domain to multidomain particles by increasing annealing time. They conclude that when we manipulating the annealing time, the crystal growth can be controlled.

A. Thakur *et al.* [42] synthesized the strontium ferrite nano particles by citrate precursor technique and preheating at 500 $^{\circ}$C for 5 h. They examined the resistivity value of the prepared sample and observed that it is increased with increase in La^{3+} concentration. They concluded that this substitution of La^{3+} on iron sites has reduced the carrier concentration, resistivity which remarkable changes in magnetic properties. They observed the saturation magnetization of La^{3+} doped ferrite to be decreased with La^{3+} content. Concluded that the coercivity can be improved by substitution of La^{3+}.They explained the enhancement in coercivity on the basis of strong magneto crystalline anisotropy. They observed that it can be used as dielectric or magnetic filler to minimize the electromagnetic interference as well as to obtain desired SNR.

A. Gruskova *et al.* [43] prepared the magnetic analysis of La–Zn substituted M-type Ba ferrites by the solgel method. Examined that it shows better remenence and saturation magnetization and coercivity than those prepared by the precursor method. Observed That remenence and saturation magnetization both are increased for samples up to x = 0.4. They found that when Zn^{2+} occupies the $4f_1$ sites, which have contribution to negative magnetic polarisation, and confirmed by slight increase of remenence and saturation magnetization at small x. They observed the H_c as a function of x, which was slowly decreases at both substitutions. They have expressed in decrement of H_c at x = 0.2. They conclude that substitutions of La^{3+} ions for Ba^{2+} ions is associated with a valence change of Fe^{3+} to Fe^{2+} ion at 2a or $4f_2$ site.

S. Verma *et al.* [44] synthesized La substituted barium hexaferrite by solid state sintering method. They investigated structural and magnetic properties by X-ray diffraction (XRD), vibrating sample magnetometer (VSM) and Mössbauer spectroscopy. They refined XRD pattern and suggest the formation of single phase hexaferrite. Analyzed that when increased La substitution (x), then saturation magnetization increased and reached maximum without any noticeable change in coercivity. They Fitted Mössbauer spectra of $Ba_{1-x}La_xFe_{12}O_{19}$ showed increase in hyperfine field and a transition from Fe ion to Fe ion at site.

CHAPTER-3 EXPERIMENTAL DETAILS

3.1 Sample Prepration:

La-doped ($Ba_{1-x}La_xFe_{12}O_{19}$) and La-dispersed ($BaFe_{12}O_{19}$) barium hexaferrite samples were prepared by solid state synthesis method. Details of sample preparation are given below:

3.1.1 Preparation of La doped and La dispersed barium hexaferrite:

To prepare La-doped and La-dispersed $BaFe_{12}O_{19}$, laboratory grade Fe_2O_3 (purity 99.0% Aldrich grade), $BaCO_3$ (purity 99.0% sigma ald rich) and La_2O_3 (purity 99.0% sigma ald rich) were used as raw materials. The stoichiometric compositions of raw powders were weighed according to the equation below:

For La substituted $BaFe_{12}O_{19}$:

$$(1-x)\ BaCO_3 + x\ La_2O_3 + 6Fe_2O_3 \longrightarrow Ba_{1-x}La_xFe_{12}O_{19} \quad (1)$$

For La dispersed $BaFe_{12}O_{19}$:

$$BaCO_3 + 6Fe_2O_3 + x\ La_2O_3 \longrightarrow BaFe_{12}O_{19} \quad (2)$$

Where; x were varied from 0.0 to 0.2.

Weighed powders were first premixed in pestle and mortar for 30 minute. Further wet mixing was done in acetone media using planetary ball milling for 3 hours at 60 rpm. The ball to charge ratio was kept 2:1. The mixed powder were dried and calcined in muffle furnace at temperature 1250°C for 3 hours. The heating and cooling rate was 5°C/minute. After calcination, the powders were wet ground for 1 hour in ball milling using tungsten carbide ball and zar. The ball to charge ratio were kept constant to 10:1. Figure 3.1 shows the flow diagram for making La-doped and dispersed $BaFe_{12}O_{19}$.

3.1.2 Characterizations:

Phase analyses of all the powders were carried out by X-Ray diffractometer X' pert PRO PAN analytical using Cu Kα radiation (λ=1.54 Å). It was done at 45 KV and 40 mA

field. For X-ray diffraction, powders were placed on sample holder and kept in XRD and applied the diffraction angle from 15^{o} to 80^{o} with step size of 0.02.

The size and shape of the particles were analyzed by scanning electron microscope JSM-6510. For SEM micrograph, preparation of powder for characterization, it were placed on a carbon tape and coated with thin layer of Au-Pd to make it conducting. The micrographs were taken in secondary electron mode and magnified at 5000X magnification at 20 volt.

The room temperature (*R-T*) magnetic properties and hyperfine parameters were measured by vibrating sample magnetometer (VSM) and Mössbauer spectroscopy respectively. Mössbauer characterizations were performed in the transmission geometry, by a ^{57}Co(Rh) source [44]. The Mössbauer spectrum was analyzed with a nonlinear least-square fitting, with Lorentzian line shape. For VSM, the powder was placed on sample holder and kept between two high magnetic field in which it start vibrating at 30 amp. Applied the maximum field was 1 T with the step size of 200 Oe.

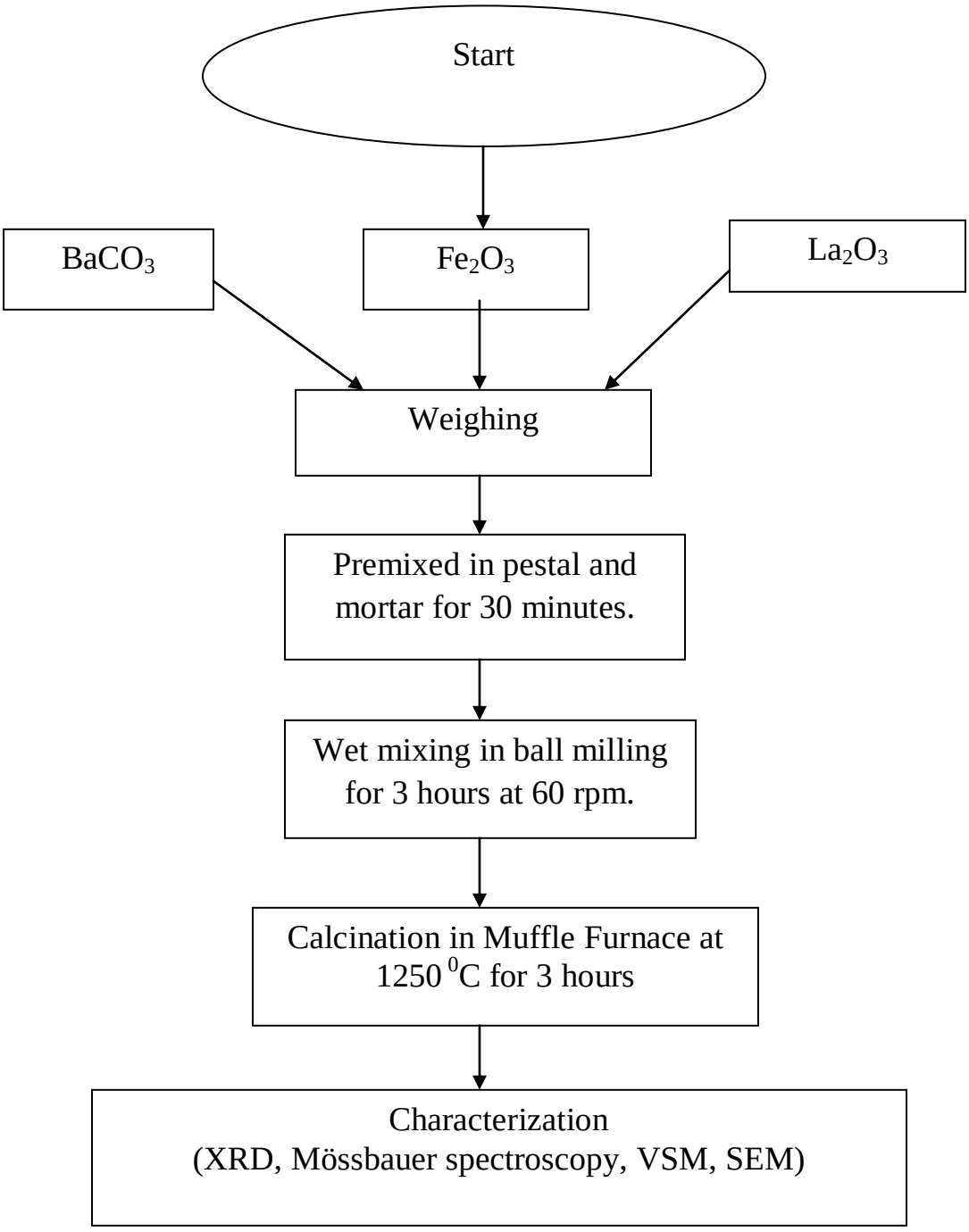

Figure 3.1 Flow chart for making La-doped and dispersed barium barium hexaferrite

4.1 Structural Characterization:

Figure 4.1 shows the X-ray diffraction pattern of pure and La-doped $BaFe_{12}O_{19}$. All powders were calciend 1250 ^{0}C for 3 hrs. The XRD patterns were matched with JCPDS card no. 43-0002. X-ray patterns show the single phase $BaFe_{12}O_{19}$ without any impurity and residual phase.

Absence of other phase suggest that La enters the hexaferrite structure in the whole range of substitution [45].

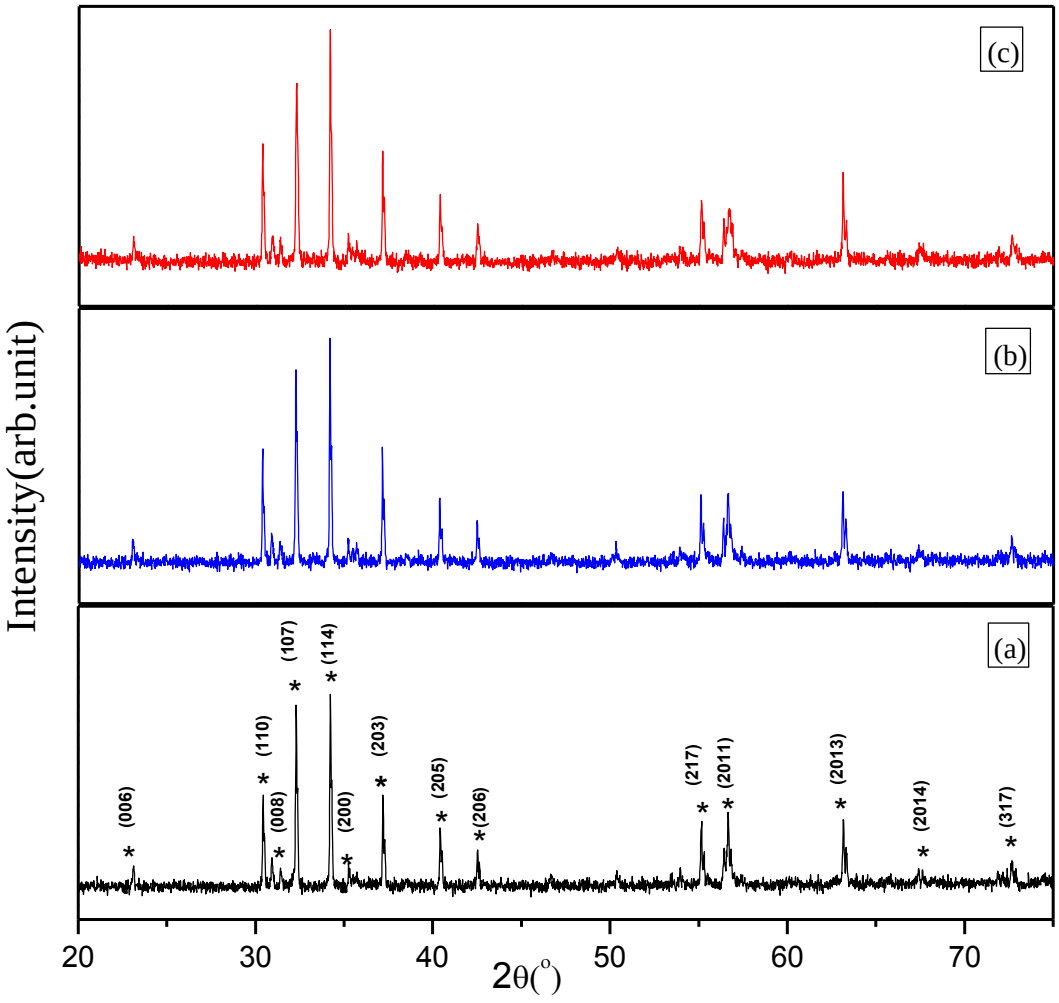

Figure 4.1 X-ray diffraction pattern (a) Pure $BaFe_{12}O_{19}$, (b) 0.1 La-doped $BaFe_{12}O_{19}$, (c) 0.2 La-doped $BaFe_{12}O_{19}$

Figure 4.2 shows the X-ray diffraction pattern of pure and La-dispersed $BaFe_{12}O_{19}$. It can be seen from the patterns that La-dispersed samples shows the emergence of secondary phase of barium monoferrite ($BaFe_2O_4$) with major phase of barium hexaferrite. No peaks of dispersed La_2O_3 was observed in the samples.

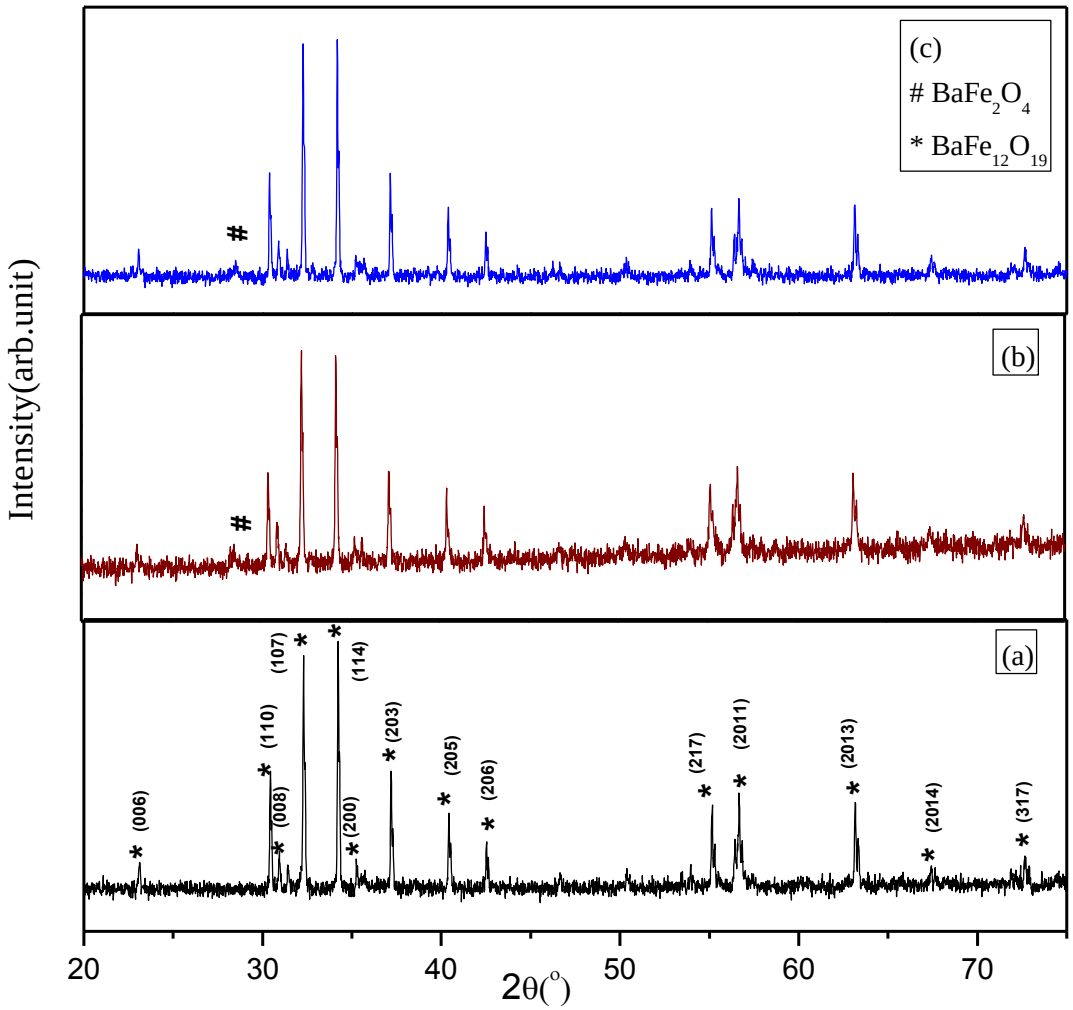

Figure 4.2 X-ray diffraction pattern (a) pure $BaFe_{12}O_{19}$, (b) 0.1 La-dispersed $BaFe_{12}O_{19}$, (c) 0.2 La-dispersed $BaFe_{12}O_{19}$

The crystallite size of $BaFe_{12}O_{19}$ calculated by Debye Scherer formula given below:

$$D = \frac{K\lambda}{\beta \cos \theta} \qquad [1]$$

Where D is the mean crystallite size, K is the shape factor, λ is the x-ray wavelength, typically 1.54 Å, β is the line broadening at half the maximum intensity (FWHM) in radians, and θ is the Bragg angle. From calculation, the crystallite sizes of all samples

were nearly constant (52.40 ± 5 nm). This suggests that dispersed La does not have any pinning effect on the particles.

4.2 Mössbauer Spectroscopy characterization:

Mössbauer spectra of pure $BaFe_{12}O_{19}$, at room temperature is shown in figure 4.3. Spectra were fitted for five discrete sextets, each sextet corresponding to one of the five different crystallographic sites, i.e., 12k ,4f1, 4f2, 2a and 2b sites, respectively. The fitted parameters were the hyperfine field (B_{hf}), the qudrupolar shift (QS), the isomer shift (δ) and the line width (Γ). It is observed that the fitted values are consistent with previously reported for the $BaFe_{12}$ O_{19} [44]. The values of hyperfine field (B_{hf}), the qudrupolar shift (QS), the isomer shift (δ) and the line width (Γ) are given in the table 4.1

.

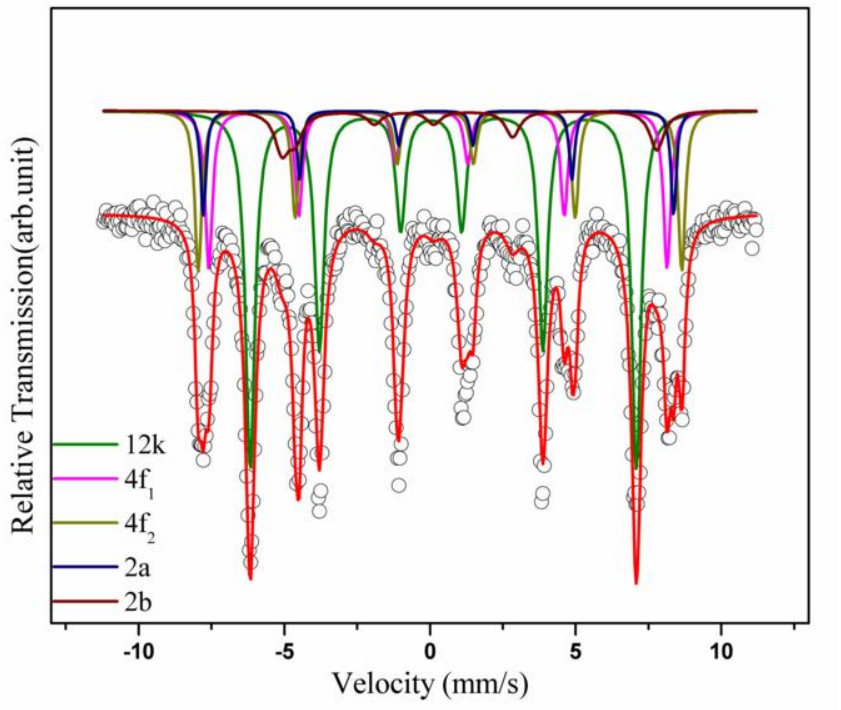

Figure4.3 Mössbauer spectra of pure $BaFe_{12}O_{19}$

Table 4.1 Hyperfine field value for pure hexaferrite

Site	IS(mm/s)	QS(mm/s)	B_{hf} (T)
12k	0.24	0.41	41.0
$4f_1$	0.16	0.21	48.7
$4f_2$	0.26	0.16	51.4
2a	0.24	0.09	50.0
2b	0.23	2.24	39.9

4.3 Magnetic measurements:

The *R-T* hysteresis loops of pure $BaFe_{12}O_{19}$ and La-substituted $BaFe_{12}O_{19}$ are shown in Fig. 4.4. The maximum applied field was 1Tesla the step of 200 Oe. The values of saturation magnetization (M_s) and coercivity (H_c) measured from the graph. The graph shows that the H_c decreases from 1624 Oe to 1458 Oe for 0.1 La-substitution and increases up to 1731 Oe for 0.2 La-substitution. H_c of $BaFe_{12}O_{19}$ primarily depends upon magnetocrystalline anisotropy and particle size [46]. As observed in SEM, particle size is nearly constant therefore H_c is nearly constant in doped $BaFe_{12}O_{19}$. M_s, decreases from 57.8 to 51.8 with increase of La-substitution. It is reported that, by partial substitution of La to Ba site, valence of Fe^{3+} changes to Fe^{2+} at 2a site by the process of magnetic dilution, therefore, the positive sign in front of the magnetic moment of 2a site become negative, as a result magnetization of samples decreases [22]. Table 4.2 shows the value of H_c, M_s and remanent magnetization (M_r).

The *R-T* hysteresis loops of pure $BaFe_{12}O_{19}$ and La-dispersed $BaFe_{12}O_{19}$ are shown in Fig. 4.5 respectively. The values of M_s and H_c measured from the graph. Figure 4.5 shows the variation in H_c with respect of pure $BaFe_{12}O_{19}$. The graph shows that the H_c remarkably decreases from 1624 Oe to 656 Oe for La-dispersed, which may be due to decrease in magnetocrystalline anisotropy with addition of La. In M_s, no such variations were showing for La-dispersed. Table 4.2 shows the value of H_c, M_s and M_r.

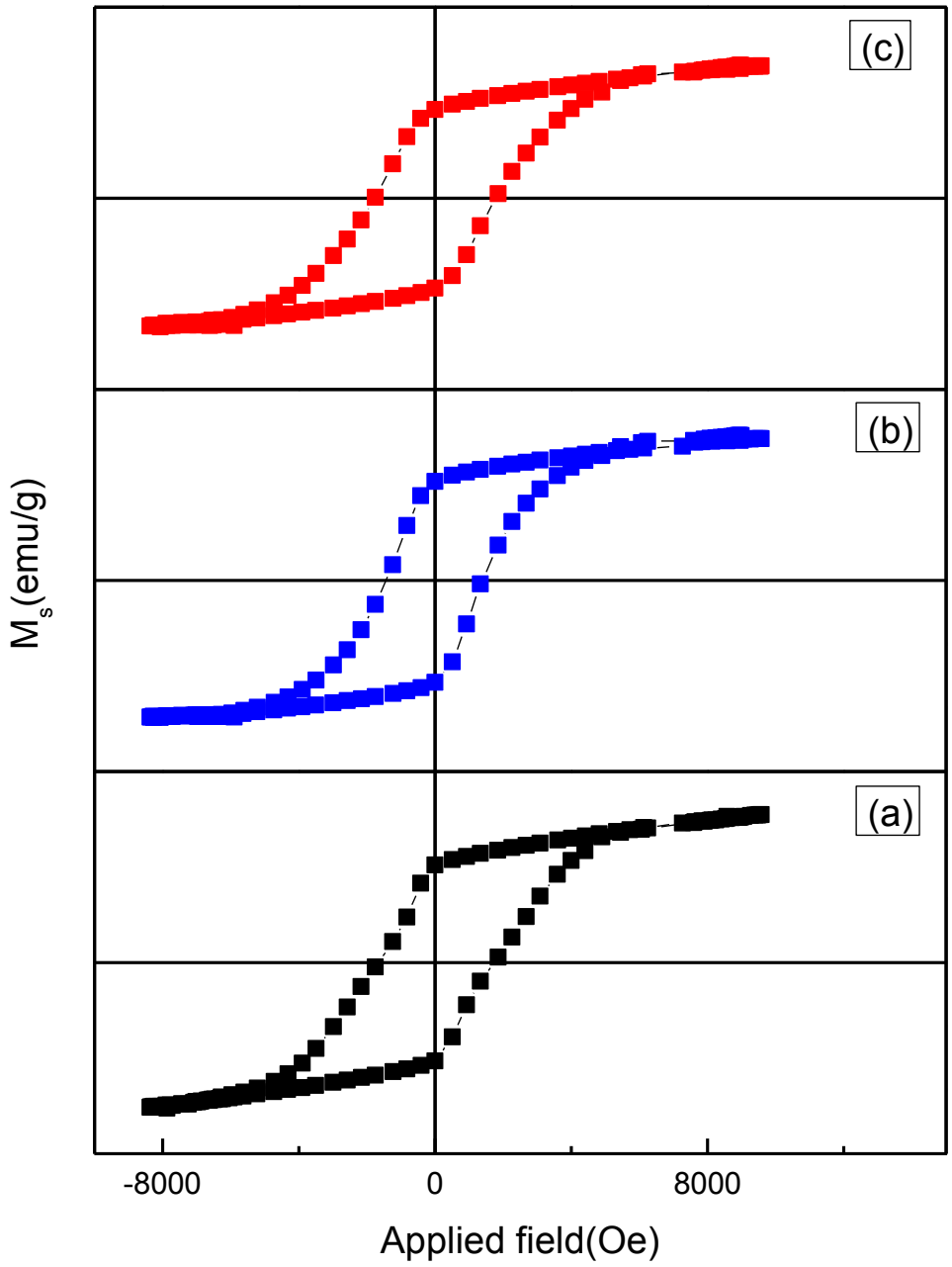

Figure 4.4 Hysteresis loop (a) pure $BaFe_{12}O_{19}$, (b) 0.1 La-doped $BaFe_{12}O_{19}$ and (c) 0.2 La-doped $BaFe_{12}O_{19}$

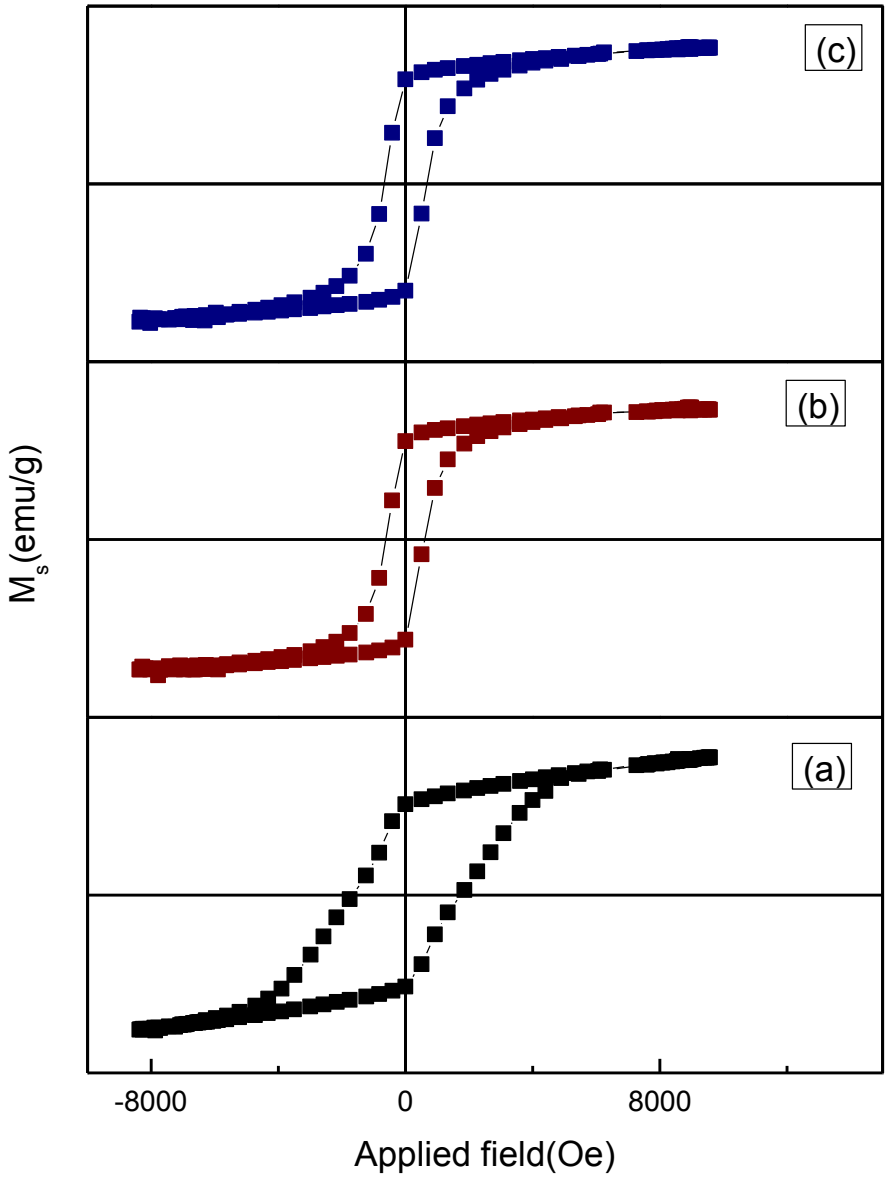

Figure 4.5 Hysteresis loop (a-pure $BaFe_{12}O_{19}$, b-0.1 La-dispersed $BaFe_{12}O_{19}$, c-0.2 La-dispersed $BaFe_{12}O_{19}$)

Fig. 4.6 shows the comparison *M-H* behavior in La-doped and La-dispersed samples. It is clearly observable that H_c is suppressed by La dispersion.

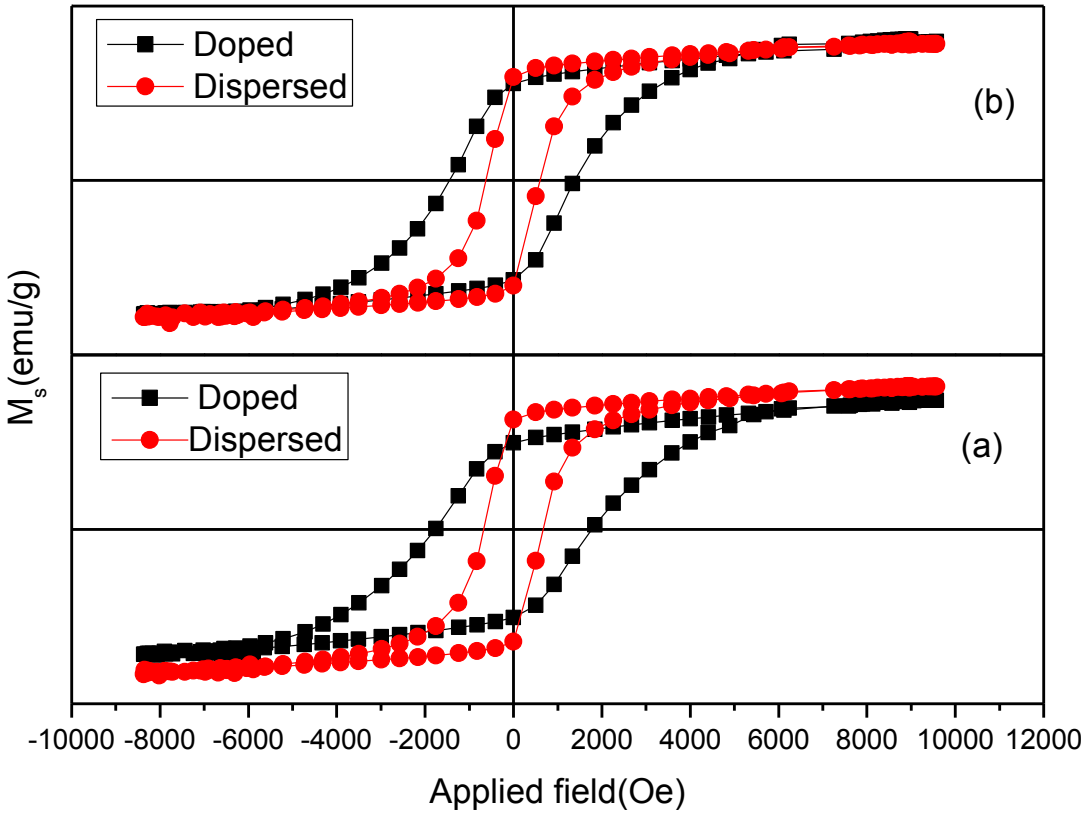

Figure 4.6 Hysteresis loop (a-0.2 La-doped and dispersed, b-0.1 La-doped and dispersed)

Table 4.2 Magnetic properties of La-doped and dispersed $BaFe_{12}O_{19}$

Sample name	***M*$_s$(emu/g)**	***M*$_r$(emu/g)**	***H*$_c$(Oe)**
$BaFe_{12}O_{19}$-pure	57.84	38.40	1624
0.1 La-doped $BaFe_{12}O_{19}$	55.77	39.02	1458
0.2 La-doped $BaFe_{12}O_{19}$	51.81	34.55	1731
0.1 La-dispersed $BaFe_{12}O_{19}$	54.85	41.39	607
0.2 La-dispersed $BaFe_{12}O_{19}$	57.38	43.99	656

4.4 Scanning Electron Microscopy:

Figure 4.7 (a-e) shows the SEM micrograph of pure $BaFe_{12}O_{19}$, La-doped and La-dispersed $BaFe_{12}O_{19}$. From micrograph, it can be seen that the shape of the particles are irregular however, some hexagonal grains is also observed. The particle size analysis was carried out on SEM micrograph by counting the particle on lines drawn over to micrograph. Particle sizes are shown in table 4.3. It is clear that average particle size is nearly constant for doped and dispersed samples.

Table 4.3 Particle size of La-doped and dispersed

Sample name	**Particle size (μm)**
$BaFe_{12}O_{19}$	1.52±0.39
0.1 La-doped $BaFe_{12}O_{19}$	1.43±0.37
0.2 La-doped $BaFe_{12}O_{19}$	1.56±0.74
0.1 La-dispersed $BaFe_{12}O_{19}$	1.24±0.44
0.2 La-dispersed $BaFe_{12}O_{19}$	1.45±0.61

Figure 4.7(a):

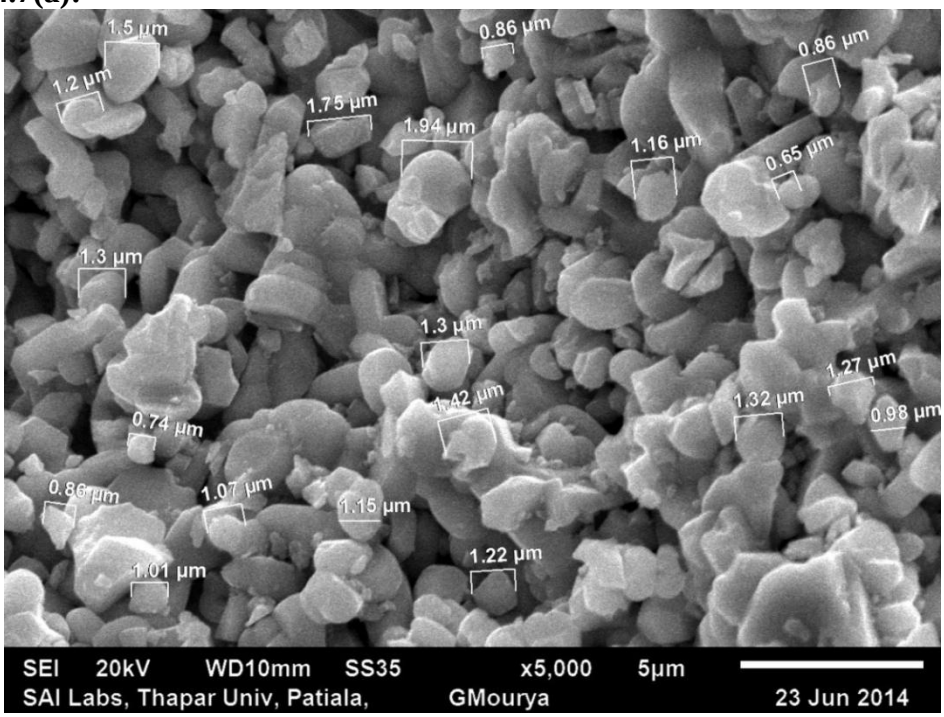

Figure:4.7(b)

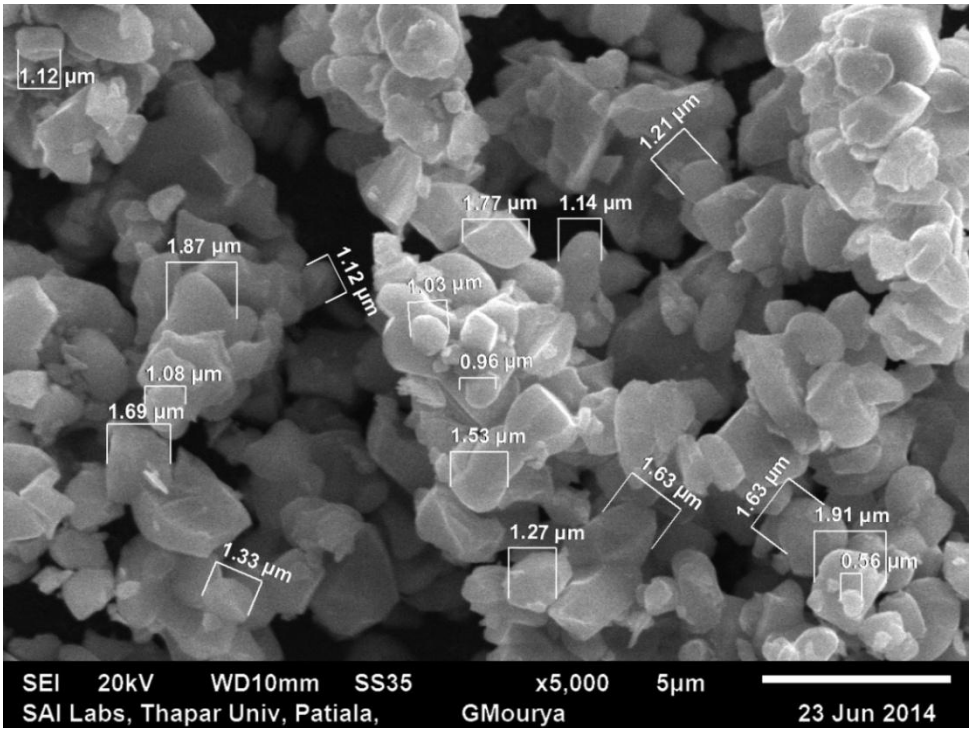

Figure 4.7(c):

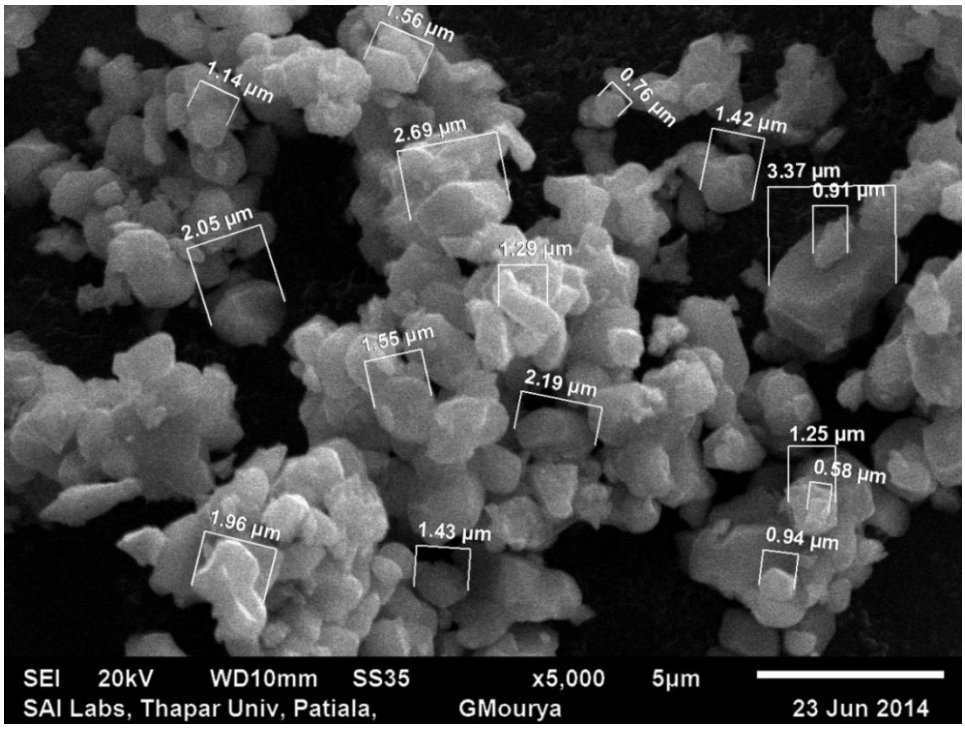

Figure 4.7(d):

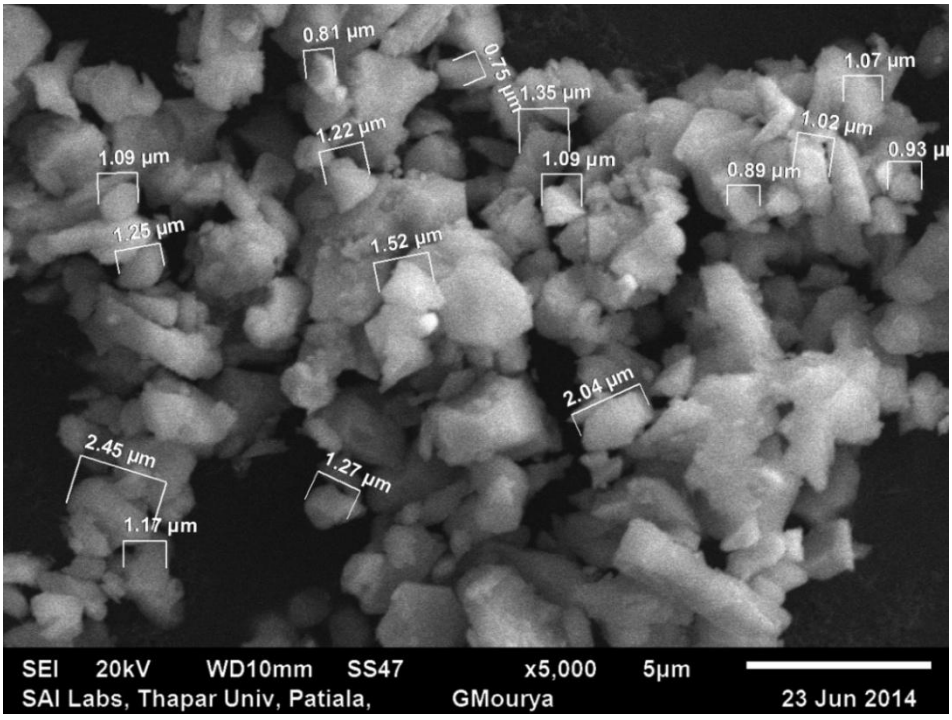

Figure 4.7(e):

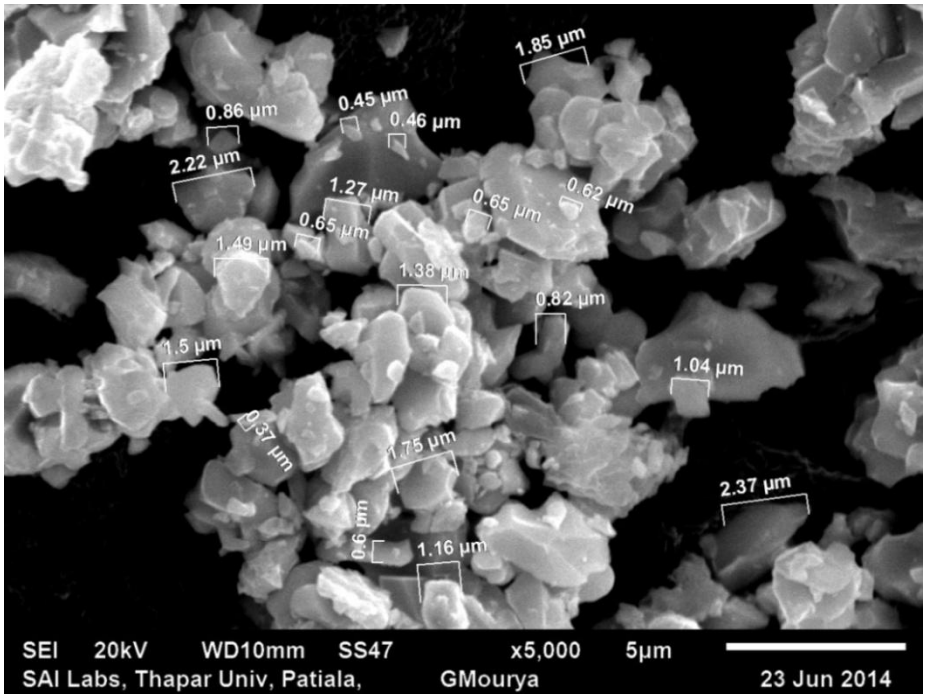

Figure 4.7: SEM micrographs (**a**- Pure $BaFe_{12}O_{19}$, **b**-0.1 La-doped $BaFe_{12}O_{19}$, **c**-0.2 La-doped $BaFe_{12}O_{19}$, **d**- 0.1 La-dispersed $BaFe_{12}O_{19}$, **e**- 0.2 La-dispersed $BaFe_{12}O_{19}$)

CHAPTER-5 CONCLUSION

La-doped $BaFe_{12}O_{19}$ and La-dispersed $BaFe_{12}O_{19}$ powders were prepared by solid state synthesis method. The powders were calcined at temperature 1250°C for 3 hours respectively. XRD pattern shows the single phase $BaFe_{12}O_{19}$ for La-doped samples, whereas for La-dispersed, some $BaFe_2O_4$ phase was found as a secondary phase. The particle size analysis was carried out by SEM micrographs. From SEM micrographs no variations is observed in particle size. From magnetic measurement, it can be concluded that La-dispersed samples have low *Hc* than La-doped and pure $BaFe_{12}O_{19}$. M_s found to decreased from 57.8 to 51.8 (emu/g) for doped samples, whereas, no remarkable variation is observed in La-dispersed. Therefore it could be concluded that low H_c $BaFe_{12}O_{19}$ can be obtained by La_2O_3 dispersion, without any change in M_s. Such dispersed candidate could be possible solution for high frequency application, where high M_s and low H_c is required.

REFERENCES

1. 'Introduction to magnetic materials' B. D. Cullity, C. D. Graham in second edition of Wiely publication (2009).

2. W. Ervens and H. Wilmesmeier, Ullmann's encyclopedia of industrial chemistry, Fifth edition, **16** (1990) 51.

3. M. A. Bohlmann, F. G. Jones *et al.* Metals Handbook, Ninth edition, **3** (1980) 639.

4. J. F. Herbest and J. J Croat, Journal of Magnetism and Magnetic Materials, **100** (1991) 78.

5. S. Hirosawa, A. Hanaki *et al.* Physics Reviews, **164** (1990) 117.

6. S. M. Abbas, A. K. Dixit *et al.* Journal of Magnetism and Magnetic Materials, **309** (2007) 20.

7. H. A. Kramers and L. Neel, Physics Reviews, **3** (1948) 137.

8. M. Shimada and S., Magnetics, IEEE Transactions on Magnetics, **35** (1999) 3154.

9. I. Wane, A. Bessaudou *et al.* Journal of Magnetism and Magnetic Materials, **211** (2000) 309.

10. M. B. Amin and J. R. James, Journal of Electroceramic, **51**(1981) 209.

11. E. W. Gorter and E. David, IEEE Transaction on Magnetic Materials, **104** (1957) 2252257.

12. P.W. Anderson and D. Stoppels, Physical Review, **79** (1957) 353.

13. Y. Goto and K. Takahashi, Japan Society of Powder and Powder Metallurgy, **17** (1971) 197.

14. F. Kamamaru, M. Shimada *et al.* Journal of Physics and Chemistry, **33** (1972) 156.

15. R. S. Meena, S. Bhattachrya *et al.* Materials Science and Engineering, **171** (2010) 133.

16. C. Mukesh, D. Subhash *et al.* IEEE Transactions on Magnetics, **42** (2006) 11.

17. A. H. Lu, E. L. Salabas *et al.* Journal of Applied Physics, **12** (2007) 1244.

18. C. J. Brinker, G. W. Scherer *et al.* Journal of Non crystalline solid, **70** (1990) 322.

19. L. L. Hench and J. K. West, Chemical Reviews, **5** (1990) 15.

20. D. Rodrigues and F. Jose, Journal of Magnetism and Magnetic Materials, **437** (1999) 53.

21. C. N. Chinnasamy, T. Sakai, *et al.* Journal of Applied Physics, **103** (2008) 07F710.

22. H. Sozeri, I. Kucuk *et al.* Journal of Magnetism and Magnetic Materials **323** (2011) 1799.

23. R. M. Kershi, M.I. Chinose *et al.* IEEE Transaction on Magnatism, **34** (1998) 1641.

24. P. Sharma, R. A. Rocha *et al.* Journal of Alloys and Compounds **443** (2007) 42.

25. M. Radawan, J. M. Le Bretona *et al.* Journal of Magnatic Material **293** (1999), 1256.

26. Y Chen, Chi Pui Li *et al.* Science and Technology of Advanced Materials **7** (2006) 846.

27. A. Ghasemi, I. Manolakis *et al.* Journal of Alloys and Compounds **427** (2007) 194.

28. S. Ounnunkad, P. Winotai *et al.* Journal of Electroceramics, **16** (2006) 361.

29. C. Li and S. W. Lee, Journal of Applied Physics, **87** (2000) 6244.

30. N. Chan, K. Haga *et al.* Journal of Magnetism and Magnetic Materials, **290** (2005) 1191.

31. R. Grossinger, M. Kupferlin *et al.* IEEE Transaction on Magnetics., **39** (2003) 2913.

32. D. Seifert, J. Topfer *et al.* Journal of Magnetic Materials., **321** (2009) 4051.

33. M. Kupferling, A.K. Dixit *et al.* Journal of Magnetism and Magnetic Materials, **309** (2007) 20.

34. V. Babu, B. Tang *et al.* Journal of Physics, **152** (2009) 012064.

35. W. Zhong, S. Y. An *et al.* Journal of Applied Physics, **87** (2000) 6244.

36. F, Hu and J. C. Jeschke, Journal of Applied Physics, **34** (1963) 1271.

37. T. T.V. Nga, N. P. Duong *et al.* Communications in Physics, **20** (2010) 142.

38. X. Liu, W. Zhong *et al.* Journal of Magnetic Materials, **238** (2002) 214.

39. R. Nowosielski, I. J. Jang *et al.* Journal of Applied Physics, **81** (1997) 4275.

40. T. Kaur, E. E. Carpenter *et al.* IEEE Transaction on Magnetics, **34** (1998) 1113.

41. C. Doroftei, E. Rezlescu *et al.* Journal of Optoelectronics And Advanced Materials, **8** (2006) 1023.

42. A. Thakur, R. R. Singh *et al.* Journal of Magnetism and Magnetic Materials, **326** (2013) 40.

43. A. Gruskova, J. Lipka *et al.* Springer Science, **164** (2005) 27.

44. S. Verma , P. Sharma *et al.* IEEE Transactions on Magnetics, **50** (2014) 42.

45. G. Litsardakis, I. Manolakis *et al.* IEEE Transactions on Magnetics, **44** (2008) 11.

46. L. Lechevallier, J. M. Le Breton *et al.* Journal of Magnetism and Magnetic Materials, **269** (2004) 192.